Breast Cancer: Early Prediction of Response to Neoadjuvant Chemotherapy Using Parametric Response Maps for MR Imaging[1]

Nariya Cho, MD
Seock-Ah Im, MD
In-Ae Park, MD
Kyung-Hun Lee, MD
Mulan Li, PhD
Wonshik Han, MD
Dong-Young Noh, MD
Woo Kyung Moon, MD

Purpose: To prospectively compare the performance of dynamic contrast material–enhanced (DCE) magnetic resonance (MR) imaging using parametric response map (PRM) analysis with that using pharmacokinetic parameters (transfer constant [K^{trans}], rate constant [k_{ep}], and relative extravascular extracellular space [v_e]) in the early prediction of pathologic responses to neoadjuvant chemotherapy (NAC) in breast cancer patients.

Materials and Methods: The institutional review board approved this study; informed consent was obtained. Between August 2010 and December 2012, 48 women (mean age, 46.4 years; range, 29–65 years) with breast cancer were enrolled and treated with an anthracycline-taxane regimen. DCE MR imaging was performed before and after the first cycle of chemotherapy, and the pathologic response was assessed after surgery. Tumor size and volume, PRM characteristics, and pharmacokinetic parameters (K^{trans}, k_{ep}, and v_e) on MR images were assessed and compared according to the pathologic responses by using the Fisher exact test or the independent-sample *t* test.

Results: Six of 48 (12%) patients showed pathologic complete response (CR) (pCR) and 42 (88%) showed nonpathologic CR (npCR). Thirty-eight (79%) patients showed a good response (Miller-Payne score of 3, 4, or 5), and 10 (21%) showed a minor response (Miller-Payne score of 1 or 2). The mean proportion of voxels with increased signal intensity (PRM_{SI+}) in the pCR or good response group was significantly lower than that in the npCR or minor response group (14.0% ± 6.5 vs 40.7% ± 27.2, $P < .001$; 34.3% ± 26.4 vs 52.8% ± 24.9, $P = .041$). Area under the receiver operating characteristic curve for PRM_{SI+} in the pCR group was 0.770 (95% confidence interval: 0.626, 0.879), and that for the good response group was 0.716 (95% confidence interval: 0.567, 0.837). No difference in tumor size, tumor volume, or pharmacokinetic parameters was found between groups.

Conclusion: PRM analysis of DCE MR images may enable the early identification of the pathologic response to NAC after the first cycle of chemotherapy, whereas pharmacokinetic parameters (K^{trans}, k_{ep}, and v_e) do not.

Clinical trial registration no. NCT01190566

[1] Form the Departments of Radiology (N.C., M.L., W.K.M.), Internal Medicine (S.A.I., K.H.L.), Pathology (I.A.P.), and Surgery (W.H., D.Y.N.), Seoul National University College of Medicine, 101 Daehak-ro, Jongno-gu, Seoul 110-744, Republic of Korea. Received June 10, 2013; revision requested August 9; final revision received December 27; accepted January 14, 2014; final version accepted January 31. Supported by the Korea Healthcare Technology R&D Project, Ministry of Health & Welfare, Republic of Korea (grants A102065-37 and A070001). **Address correspondence to** W.K.M. (e-mail: *moonwk@ snu.ac.kr*).

Neoadjuvant chemotherapy (NAC) has been increasingly utilized in the treatment of breast cancer, as the long-term distant and local-regional control of cancer provided by NAC have been reported to be similar to those offered by adjuvant chemotherapy (1,2). Although approximately 80% of patients respond to NAC, with 6%–25% of patients showing a pathologic complete response (CR) (pCR), 20% of patients remain resistant to chemotherapy (3,4). Therefore, predicting the response such that treatment can be modified in both responders and nonresponders at an earlier time is highly important.

Researchers in several studies have reported that reductions in the transfer constant (K^{trans}) or the rate constant (k_{ep}) obtained after two cycles of NAC were associated with the response to NAC (5,6) and better survival outcomes (7). However, the measurement of K^{trans} may be too complicated to use in real clinical practice as a magnetic resonance (MR) imaging protocol that uses high temporal resolution with a trade-off in spatial resolution and T1 mapping. Indeed, researchers in the recent multi-institutional American College of Radiology Imaging Network 6657 trial investigating the effectiveness of dynamic contrast material–enhanced (DCE) MR imaging for the prediction of the response to NAC did not analyze K^{trans} but rather used acquisitions at three times because of the difficulty in standardizing imaging protocols from multiple institutions (8). Voxel-based parametric response map (PRM) analysis of DCE MR images has been shown to be accurate for early prediction of the effectiveness of chemotherapy–radiation therapy in brain glioma (9,10), of transarterial chemoembolization in hepatocelluar carcinoma (11), and of NAC in breast cancer (12). However, to our knowledge, no reports have addressed PRM analysis for breast cancer patients after the first cycle of NAC. We hypothesized that PRM analysis would be as predictive of the response as pharmacokinetic parameters, while it is more readily applicable in real clinical practice. Thus, the purpose of this study was to prospectively compare the performance of DCE MR imaging using PRM analysis with that using pharmacokinetic parameters (K^{trans}, k_{ep}, and v_e) in the early prediction of pathologic responses to NAC in breast cancer patients.

Advance in Knowledge

- In breast cancer, patients receiving neoadjuvant chemotherapy (NAC), volumetric assessment of signal intensity changes by using a three-dimensional registration program for dynamic contrast-enhanced (DCE) MR imaging prior to treatment and after the first cycle of chemotherapy resulted in the prediction of subsequent pathologic complete response (pCR), with an area under the receiver operating characteristic curve of 0.770 (95% confidence interval: 0.626, 0.879).

Materials and Methods

Siemens Medical Solutions (Erlangen, Germany) provided the software (MR Oncotreat and Tissue4D) used in this study. However, no authors were funded by Siemens Medical Solutions, and the authors had complete control of the data and information submitted for publication.

Patients and Treatment

This prospective study was conducted with institutional review board approval of Seoul National University Hospital (Seoul, Korea). Written informed consent was obtained from all patients, and the study was registered in *ClinicalTrials.gov* (registration no. NCT01190566) prior to patient enrollment. Between August 2010 and December 2012, 57 patients with stage II or stage III breast cancer who received NAC were enrolled. As defined in a previous study (13), the eligibility criteria were as follows: *(a)* breast cancer was pathologically confirmed by means of core needle biopsy; *(b)* the patient had initial clinical stage II or III breast cancer; *(c)* the lesion was objectively measurable; *(d)* the patient had an Eastern Cooperative Oncology Group performance score of 0–2; *(e)* the patient was previously untreated; and *(f)* the patient had adequate bone marrow and hepatic, cardiac, and renal function. The patients received six cycles of neoadjuvant docetaxel (Taxotere; Sanofi Aventis, Paris, France), 75 mg/m^2, with doxorubicin (Adriamycin PFS; Ildong Pharmaceutical, Seoul, Korea), 50 mg/m^2, or four cycles of doxorubicin (60 mg/m^2) with cyclophosphamide (Endoxane;

Implication for Patient Care

- DCE breast MR imaging with parametric response map analysis using pre- and posttreatment image coregistration may help to identify breast cancer patients who would show a pCR to NAC after the first chemotherapy session.

Published online before print
10.1148/radiol.14131332 **Content codes:** BR MR BQ

Radiology 2014; 272:385–396

Abbreviations:
CR = complete response
DCE = dynamic contrast enhanced
ER = estrogen receptor
HER2 = human epidermal growth factor 2
k_{ep} = rate constant
K^{trans} = transfer constant
NAC = neoadjuvant chemotherapy
npCR = nonpathologic CR
pCR = pathologic CR
PR = progesterone receptor
PRM = parametric response map
PRM_{SI-} = PRM of proportions of voxels with decreased SI
PRM_{SI+} = PRM of proportions of voxels with increased SI
PRM_{SI0} = PRM of proportions of voxels with unchanged SI
ROC = receiver operating characteristic
ROI = region of interest
SI = signal intensity
3D = three-dimensional
v_e = relative extravascular extracellular space

Author contributions:
Guarantors of integrity of entire study, N.C., W.K.M.; study concepts/study design or data acquisition or data analysis/interpretation, all authors; manuscript drafting or manuscript revision for important intellectual content, all authors; approval of final version of submitted manuscript, all authors; literature research, N.C., S.A.I., W.K.M.; clinical studies, N.C., S.A.I., I.A.P., K.H.L., W.H., D.Y.N., W.K.M.; experimental studies, M.L.; statistical analysis, N.C.; and manuscript editing, N.C., W.K.M.

Clinical trial registration no. NCT01190566

Conflicts of interest are listed at the end of this article.

Baxter, Deerfield, Ill), 600 mg/m^2, followed by four cycles of docetaxel (75 mg/m^2). The regimen was administered by means of intravenous infusion every 3 weeks for each cycle, together with granulocyte colony-stimulating factor as the primary prophylaxis; this regimen was the standard preoperative schedule in our institution. The patients were evaluated clinically before each cycle of chemotherapy, and the regimen was considered to be complete when there was no evidence of progression. At the completion of chemotherapy, the patients were reevaluated with regard to their response and underwent curative surgery.

All patients underwent a DCE MR imaging examination twice: One examination was performed within 3 weeks prior to chemotherapy, and a second examination was performed 2 weeks after the first cycle of chemotherapy but prior to the second cycle of chemotherapy.

MR Imaging Technique and Image Analysis

All MR examinations were performed by using a 3.0-T imager (Verio; Siemens Medical Solutions) and a dedicated 16-channel breast coil, with patients in the prone position. The protocol included the following sequences: *(a)* a bilateral transverse fat-suppressed T2-weighted turbo spin-echo sequence (repetition time msec/echo time msec, 2500/208; section thickness, 1.5 mm; intersection gap, none; field of view, 320 mm; and matrix, 320 × 238); *(b)* a nonenhanced transverse T1-weighted three-dimensional (3D) fast low-angle shot sequence (3.4/1.4; section thickness, 2 mm; intersection gap, none; field of view, 320 mm; and matrix, 256 × 195) for measurement of the tissue T1 relaxation rate from the signal intensity (SI) of three images with 2°, 8°, and 15° flip angles; and *(c)* a dynamic transverse T1-weighted 3D fast low-angle shot sequence (3.4/1.4; flip angle, 20°; section thickness, 2 mm; intersection gap, none; field of view, 320 mm; matrix, 256 × 195; temporal resolution, 10 seconds; and acquisition time, 7 minutes 30 seconds) with a total of three phases of nonenhanced and 42 phases of contrast material–enhanced images. Gadobutrol (Gadovist; Bayer Schering Pharma, Berlin, Germany) was injected into the antecubital vein by using an automated injector (Spectris MR; Medrad Europe, Maastricht, the Netherlands) at a dose of 0.1 mmol per kilogram of body weight and at a rate of 3 mL/sec, followed by a 20-mL saline flush for all patients.

For evaluation of the overall extent of the lesion, a delayed sagittal T1-weighted 3D fast low-angle shot sequence (4.9/1.9; flip angle, 10°; section thickness, 1.5 mm; intersection gap, none; field of view, 240 mm; and matrix, 512 × 287) was performed following acquisition of the dynamic image.

The tumor size was measured as the greatest extent of the enhancing lesion on early transverse contrast-enhanced MR images. The section and direction for tumor size measurement were recorded, and the same section and direction were used for the images obtained after chemotherapy. For tumor volume and PRM analysis, Digital Imaging and Communications in Medicine files for the DCE MR images were transferred to computer software (MROncoTreat; Siemens Medical Solutions) for 3D intra- and interstudy registration and semiautomatic 3D segmentation. Images of the early contrast enhancement (90 seconds after the beginning of the contrast agent injection) phase were chosen for the analysis, as the guidelines for optimal clinical breast MR imaging recommend an early phase of less than 2 minutes (14). Nonlinear automatic registration was performed to correct for motion on the nonenhanced, early enhancement, and delayed enhancement (7 minutes after the beginning of the contrast agent injection) T1-weighted images for each image obtained prior to treatment and after the first cycle of chemotherapy. All MR images were aligned by using the early phase images as reference. The quality of registration could be evaluated with the toggle view, blended volume visualization, or checkerboard view tools, which allowed visual comparison between pre- and postregistration images, in the software. When misregistration was found, it was possible to manually adjust the pre- and postregistration images relative to each other. We performed manual adjustment in three of 48 women. No cases were excluded because of misregistration. For tumor margin segmentation, regions of interest (ROIs) were manually drawn and modified by using an interactive segmentation technique (15); two radiologists in consensus (W.K.M. and N.C., with 15 and 10 years of experience in interpreting breast MR images, respectively) performed this task. The ROIs were made as large as possible to include the entire tumor and to exclude normal breast parenchyma or fat tissue at each cross-sectional plane. The size of each ROI ranged from 0.2 cm to the maximal tumor dimension (mean, 5.0 cm; range, 1.5–11.5 cm) at each plane. The tumor volume was calculated by summing voxels with an SI enhancement of more than 50%; this threshold for comparison between nonenhanced and early contrast-enhanced images was established in another study in the NAC setting (16). The percentage of enhancement, or E, was defined in an equation, as follows: $E = [(SI_{ear} - SI_{non})/SI_{non}] \cdot 100$, where SI_{ear} is early contrast-enhanced SI and SI_{non} is nonenhanced SI.

For PRM analysis, the software calculated the interval change of SI that was based on a voxel-to-voxel comparison between SI measurements at baseline, SI_{base}, and after the first cycle of chemotherapy, $SI_{post1st}$, thus: $(SI_{post1st} - SI_{base})/SI_{base} \cdot 100$. The PRMs of proportions of voxels with increased SI (PRM_{SI+}), decreased SI (PRM_{SI-}), or unchanged SI (PRM_{SI0}) within a tumor were analyzed, and a threshold of 10% enhancement was applied. For multiple lesions, the sum of the values for the five largest lesions in each patient was calculated.

For pharmacokinetic analysis, the Digital Imaging and Communications in Medicine files from DCE MR imaging were transferred to computer software (Tissue4D; Siemens Medical Solutions). The enhancement kinetics were analyzed on the basis of the two-compartmental pharmacokinetic model described by Tofts (17) and Tofts et al (18). The concentration of the tissue contrast agent as a function of time, $C_t(t)$, was calculated according to the

following equation: $C_t(t) = (1/T1(t) - 1/T1_0)/r1$. Here, T1 ($t$) represents the tissue T1 relaxation rate at time t following the administration of the contrast agent, $T1_0$ represents the tissue T1 relaxation rate prior to contrast agent administration, and r1 represents the longitudinal relaxivity of the contrast agent, which is taken to be 5.0 $(L \cdot mmol^{-1})/sec$ for gadobutrol (19). To accurately convert the change in SI to the concentration of the contrast agent in the tissue, $C_t(t)$, the nonenhanced tissue T1 relaxation rates were obtained from the SIs of three images that were acquired with flip angles of 2°, 8°, and 15° by using the variable flip angle method (20). The tissue contrast as a function of time, $C_t(t)$, depends on the arterial blood plasma concentration, $C_p(t)$, and the arterial input function. Mathematical simulation–based fast-mode arterial input function in the computer software (Tissue4D; Siemens Medical Solutions) was used (21). An equation was calculated thus: $dC_t/dt = K^{trans}(C_p - C_t/v_e) = K^{trans} C_p - k_{ep} C_t$.

The transfer constant (K^{trans}, the constant for the transfer of the contrast agent from the plasma compartment into the extracellular extravascular space, in per minute), the extracellular extravascular space per unit volume of tissue (v_e values ranging from zero to one), and the rate constant (k_{ep}, the rate constant of the escape of the contrast agent from the extracellular extravascular space into the plasma compartment, as K^{trans}/v_e, in per minute) were derived from the time-concentration curve by using a nonlinear Levenberg-Marquardt least-squares–fitting algorithm. For measurement of the perfusion parameter of the tumor, ROIs were manually drawn in each section of the tumor in the largest dimension to cover the whole volume of the tumor. The enhancement kinetics from each pixel were measured throughout the time course of data acquisition and fitted with the pharmacokinetic model. The K^{trans}, k_{ep}, and v_e values of the whole tumor were calculated and displayed in 256-color mapping images, and the mean and median values were generated for each parameter.

Histopathologic Assessment and Response to Chemotherapy

After surgery, the pretreatment core biopsy and surgical specimens were evaluated with regard to their chemotherapy response. The *pCR* was defined as the absence of invasive tumor cells (ductal carcinoma in situ may have been present). The residual tumor size was measured with regard to invasive and in situ carcinoma components. The Miller-Payne system was also used to assess the tumor response on the basis of the reduction of tumor cellularity (22,23). A *good pathologic response* was defined as a decrease of at least 30% in the number of tumor cells relative to the pretreatment core biopsy (ie, with Miller-Payne grades of 3, 4, or 5) (23). A *minor response* was defined as a decrease of less than 30% in the number of tumor cells (ie, Miller-Payne grades of 1 or 2) (23). A *pCR* was defined as a tumor response with a grade of 5. The expression of the estrogen receptor (ER), progesterone receptor (PR), and human epidermal growth factor receptor 2 (*HER2*) was evaluated. A cutoff value of 10% was used to define positivity for the ER and PR at a magnification of ×10. *HER2* expression was initially scored as 0, 1+, 2+, or 3+ by using immunohistochemical staining. Tumors with a score of 3+ were classified as *HER2* positive, and tumors with a score of 0 or 1+ were classified as negative. In tumors with a score of 2+, gene amplification by using fluorescence in situ hybridization was used to determine the *HER2* status. *HER2* expression was considered positive if the ratio of *HER2* gene copies to chromosome 17 signals was greater than 2.2 (24). The immunohistochemical subtype of the tumor was classified as hormone receptor positive (ER positive or PR positive), triple negative (hormone receptor negative and *HER2* negative), or *HER2* positive (*HER2* positive and hormone receptor negative).

Statistical Analysis

Sample size was calculated a priori for the primary outcome measurement of PRM of proportions of voxels with increased SI by using the power analysis program (25). Assuming the proportion of pCR was 20% and to detect a minimal PRM_{SI+} difference of 20% with a standard deviation of 20% between pCR and nonpathologic CR (npCR) groups, a total of 52 patients (10 patients with pCR and 42 patients with npCR) were needed to achieve 80% power at a two-sided 5% significance level. Therefore, in the consideration of potential dropouts, we recruited a total of 57 patients.

Clinicopathologic variables and imaging variables were compared among the pCR, npCR, the good response, and the minor response groups, by using the Fisher exact test (age at diagnosis; clinical stage; expression of ER, PR, *HER2*, and Ki-67; immunohistochemical subtype; chemotherapy regimen; and type of surgery) and the independent-sample t test (tumor size, tumor volume, PRM_{SI+}, PRM_{SI-}, PRM_{SI0}, K^{trans}, k_{ep}, and v_e). We also assessed statistical power by means of post hoc power analysis. In addition, we evaluated the association between pathologic response and significant parameters stratified according to immunohistochemical subtype. Statistical analysis was not applicable for the hormone receptor–positive or *HER2*-positive subgroups, as only one patient achieved pCR in each of these subgroups.

To evaluate the contribution of a parameter to the prediction of a pCR or a good response, the area under the receiver operating characteristic (ROC) curve was analyzed. Because the PRM_{SI-} was inversely correlated with the PRM_{SI+}, we included only the PRM_{SI+} data in the ROC analysis. To suggest optimal criteria for prediction, the best cutoff value to achieve the maximal sum of the sensitivity (proportion of pathologic responders correctly classified as responders) and specificity (proportion of pathologic nonresponders correctly classified as nonresponders) was determined. The leave-one-out cross-validation analysis was performed to confirm validity of the best cutoff points of significant MR imaging parameters. All statistical analyses were performed by using software (SPSS, version 19.0,

Table 1

Association between Clinicopathologic Characteristics and Pathologic Response

Variable	pCR Group ($n = 6$)	npCR Group ($n = 42$)	*P* Value	Good Response Group ($n = 38$)	Minor Response Group ($n = 10$)	*P* Value
Age at diagnosis			.609			>.99
≤40 y	2 (18)	9 (82)		9 (82)	2 (18)	
>40 y	4 (11)	33 (89)		29 (78)	8 (22)	
Clinical stage			.591			>.99
II	2 (20)	8 (80)		8 (80)	2 (20)	
III	4 (11)	34 (89)		30 (79)	8 (21)	
ER			.073			.081
Negative	5 (24)	16 (76)		14 (67)	7 (33)	
Positive	1 (4)	26 (96)		24 (89)	3 (11)	
PR			>.99			>.99
Negative	5 (14)	31 (86)		28 (78)	8 (22)	
Positive	1 (8)	11 (92)		10 (83)	2 (17)	
HER2			>.99			.675
Negative	5 (14)	32 (86)		30 (81)	7 (19)	
Positive	1 (9)	10 (91)		8 (73)	3 (27)	
Ki-67			.179			>.99
≤14%	2 (7)	28 (93)		24 (80)	6 (20)	
>14%	4 (22)	14 (78)		14 (78)	4 (22)	
Immunohistochemical subtype			.073			.128
Hormone receptor positive	1 (4)	26 (96)		24 (89)	3 (11)	
Triple negative	4 (29)	10 (71)		10 (71)	4 (29)	
HER2 positive	1 (14)	6 (86)		4 (57)	3 (43)	
Chemotherapy regimen			.656			
Docetaxel-doxorubicin therapy	4 (11)	31 (89)		26 (74)	9 (26)	.248
Doxorubicin-cyclophosphamide plus docetaxel therapy	2 (15)	11 (85)		12 (92)	1 (8)	
Type of surgery			.651			>.99
Breast conserving	3 (10)	28 (90)		24 (77)	7 (23)	
Total mastectomy	3 (18)	14 (82)		14 (82)	3 (18)	

Note.—Data are numbers of patients. Numbers in parentheses are percentages. Percentages were rounded.

SPSS, Chicago, Ill; SAS, version 9.2, SAS Institute, Cary, NC; MedCalc, version 10.3.0, MedCalc Software, Mariakerke, Belgium; and G*Power, version 3.0.10, *http://www.gpower.hhu.de/* [25]). A difference with $P < .05$ was defined as significant.

Results

Patients and Response

Of the 57 patients enrolled, nine patients were excluded because of withdrawal of consent ($n = 3$), an inconsistent MR protocol ($n = 4$), or withdrawal from surgery ($n = 2$). Thus, 48 patients (mean age, 46.4 years; range, 29–65 years) with invasive breast cancer (mean size, 5.0 cm; range, 1.5–11.5 cm) comprised our study group (Table 1). Most of these patients had invasive ductal carcinomas that were not otherwise specified (96%, 46 of 48) and a clinical stage of II (21%, 10 of 48) or III (79%, 38 of 48). The median interval between baseline MR examination and initiation of NAC was 5 days (range, 1–19 days), and the median interval between baseline and the second MR examination was 21 days (range, 13–36 days). The median number of cycles of chemotherapy was six (range, 4–8). Two patients exhibited clinical progression during chemotherapy and underwent mastectomy after the fourth round of NAC (Fig 1).

Of the 48 patients evaluated, six patients (12%) achieved pCR (Miller-Payne grade of 5) and 42 (88%) showed npCR (Fig 2). On the basis of the Miller-Payne system, 38 patients (79%) showed a good response, with a grade of 3, 4, or 5, and the remaining 10 patients (21%) demonstrated a minor response, with a grade of 1 or 2.

With regard to clinicopathologic characteristics, no differences were observed between the pCR and npCR groups or the responders and nonresponders in terms of age; clinical tumor stage; expression of ER, PR, *HER2*, or Ki-67; immunohistochemical subtype; chemotherapy regimen; or type of surgery (Table 1). The triple-negative

Figure 1

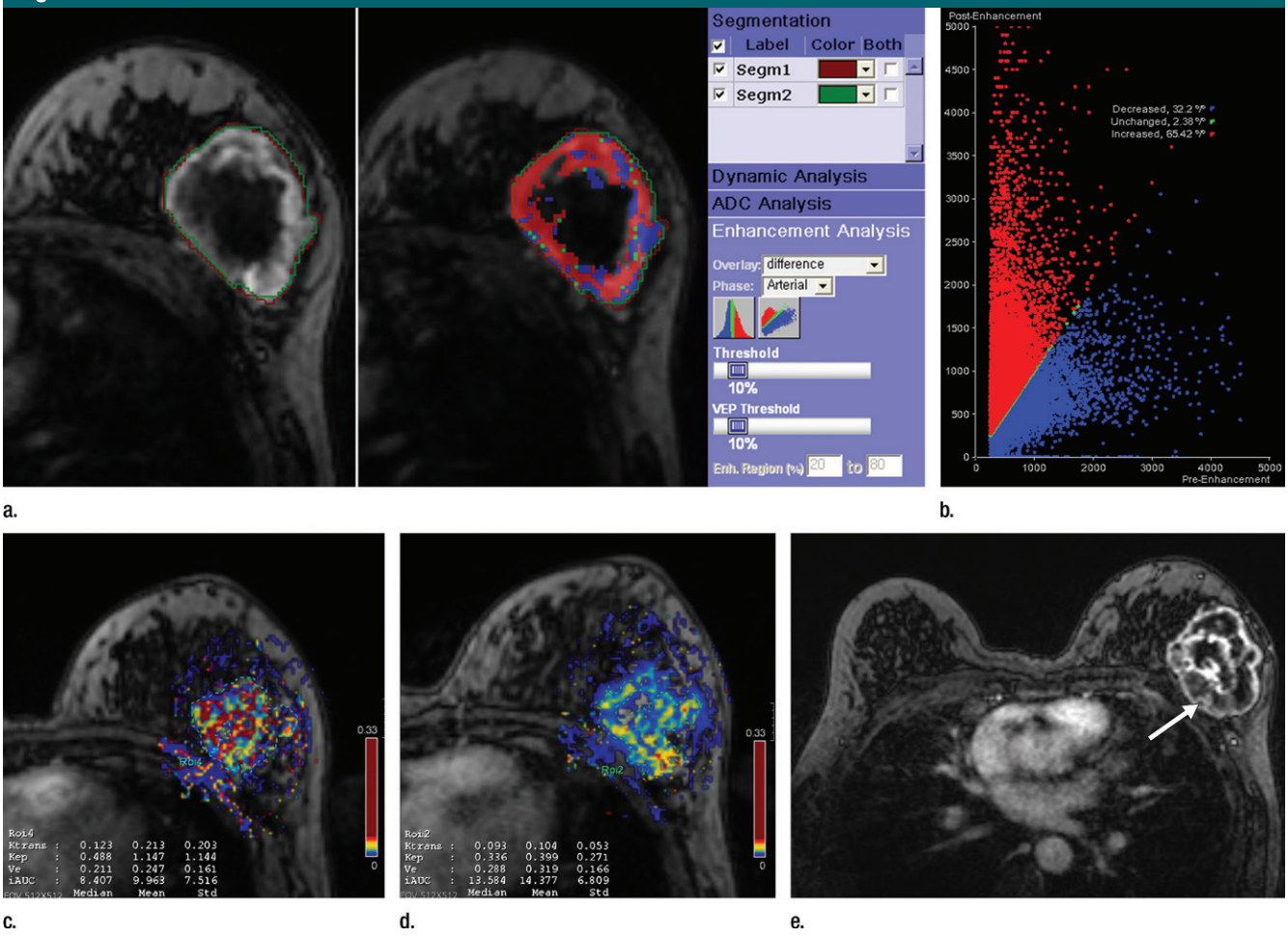

Figure 1: Invasive ductal carcinoma (ER, PR, and *HER2* negative) in a 44-year-old woman in the npCR group after NAC. **(a)** Left: PRM of baseline MR image. Middle: Contrast-enhanced T1-weighted MR image after the first cycle of chemotherapy. Image shows color-coded ROI (arrow) superimposed on a 5.5-cm enhancing mass. Orange line = margin of the tumor on the baseline MR image, green line = margin of the tumor after the first cycle of chemotherapy. Right: Screenshot of enhancement analysis work flow controls. **(b)** Scatterplot shows SI changes of voxels within the ROI before and after the first cycle of chemotherapy. Voxels with decreased, unchanged or increased SI at a 10% threshold for the entire tumor volume are displayed as red, green, or blue dots, respectively. In this patient, the proportion of voxels with increased SI was 65.42%, the proportion of unchanged voxels was 2.38%, and the proportion of voxels with decreased SI was 32.2%. **(c)** Baseline K^{trans} map shows a mass with a mean K^{trans} of 0.217 min^{-1}. The color bar indicates color codings of K^{trans} values within the map. **(d)** K^{trans} map after the first cycle of chemotherapy shows a mass with a mean K^{trans} of 0.237 min^{-1}. As the software program (Tissue4D; Siemens Medical Solutions) does not provide two-dimensional registration between baseline and posttreatment images, the measurement of K^{trans} is slightly misregistered. **(e)** K^{trans} map after the fourth cycle of chemotherapy shows that the mass (arrow) increased in size from 5.5 cm to 6.4 cm. The patient underwent surgery without completion of chemotherapy, and surgical histopathologic examination revealed a 7.0-cm invasive ductal carcinoma.

subtype tended to exhibit a higher rate of pCR (29%, four of 14) than the hormone receptor–positive (4%, one of 27) or *HER2*-positive (14%, one of seven) subtypes, but this difference was not significant ($P = .073$) (Table 1). Statistical power for the proportions of pCR between the triple-negative subtype versus the hormone receptor–positive or *HER2*-positive subtype by using post hoc power analysis was 46.2% at a two-sided 5% significance level (25).

Predictors of the Response after the First Cycle of NAC

Following the first cycle of chemotherapy, the mean tumor size had decreased in 10.4% ± 12.2 (standard deviation) of patients, and the mean tumor volume had decreased in 17.2% ± 55.0 of patients. There was no difference between the pCR and npCR groups or the good response and minor response groups at baseline or after the first cycle of chemotherapy with regard to the percentage change in mean tumor size, tumor volume, K^{trans}, k_{ep}, or v_e (Table 2). However, the mean PRM_{SI+} of the pCR group was significantly lower than that of the npCR group (14.0% ± 6.5 vs 40.7%

Figure 2

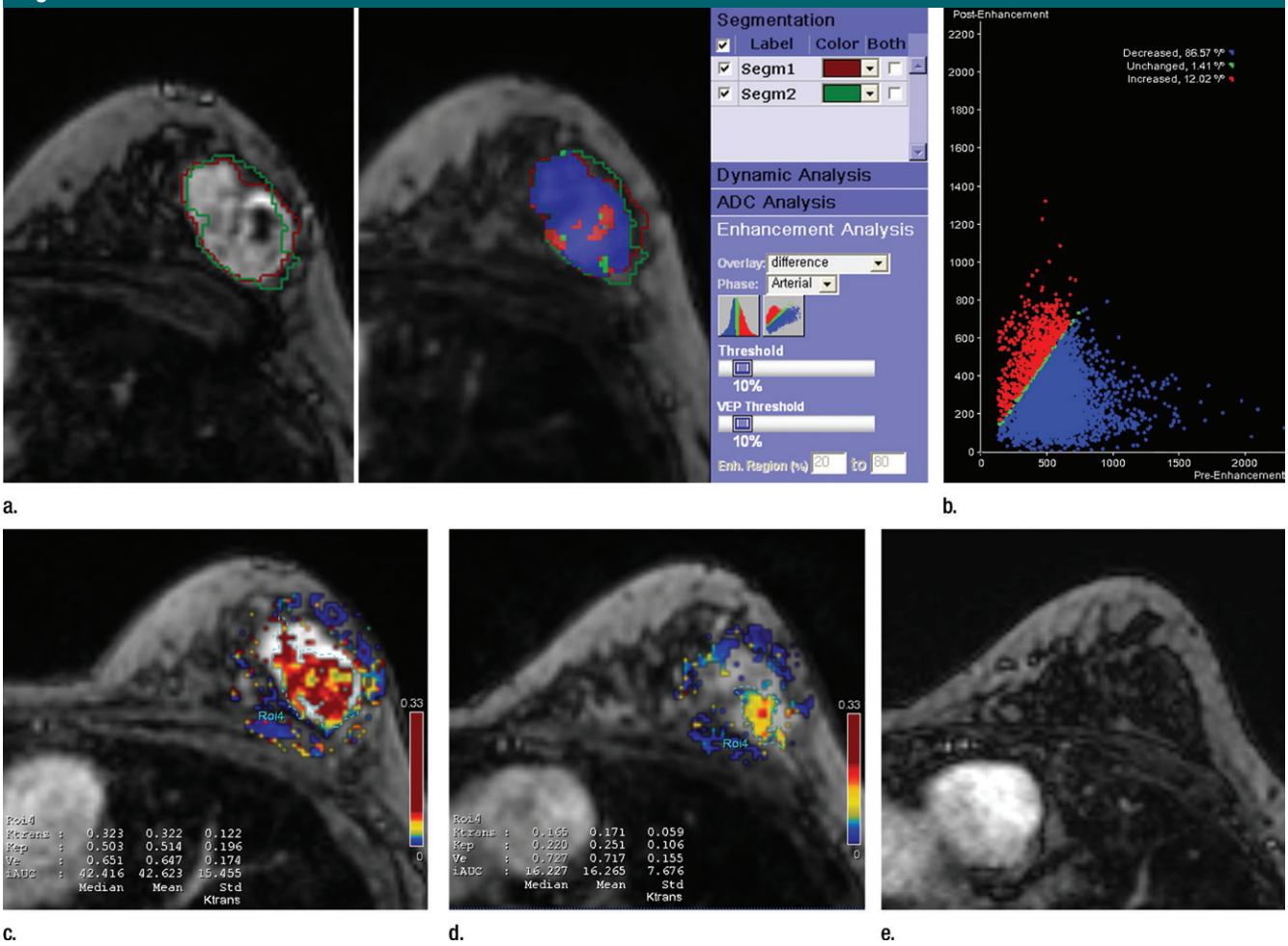

Figure 2: Invasive ductal carcinoma (ER, PR, and *HER2* negative) in a 38-year-old woman in the pCR group after NAC. **(a)** Left: PRM of baseline image. Middle: Contrast-enhanced T1-weighted MR image after the first cycle of chemotherapy. Image shows color-coded ROI superimposed on a 3.6-cm enhancing mass. Orange line = margin of the tumor on the baseline MR image, green line = margin of the tumor after the first cycle of chemotherapy. Right: Screenshot of enhancement analysis work flow controls. **(b)** Scatterplot shows SI changes of voxels within the ROI before and after the first cycle of chemotherapy. Voxels with decreased, unchanged, or increased SI at a 10% threshold for the entire tumor volume are displayed as red, green, or blue dots, respectively. In this patient, the proportion of voxels with increased SI was 12.02%, the proportion of unchanged voxels was 1.41%, and the proportion of voxels with increased SI was 86.57%. **(c)** Baseline K^{trans} map shows a mass with a mean K^{trans} of 0.329 min^{-1}. The color bar indicates color codings of K^{trans} values within the map. **(d)** K^{trans} map after the first cycle of chemotherapy shows a mass with a mean K^{trans} of 0.309 min^{-1}. **(e)** K^{trans} map after the sixth cycle of chemotherapy shows that the mass had disappeared (arrow). The patient underwent surgery, and surgical histopathologic examination revealed no residual carcinoma.

± 27.2, $P < .001$) (Table 2) (Fig 3). In addition, the mean PRM_{SI+} of the good response group was lower than that of the minor response group (34.3% ± 26.4 vs 52.8% ± 24.9, $P = .041$). With regard to the immunohistochemical subtype, the mean PRM_{SI+} of the pCR group ($n = 4$) was significantly lower than that of the npCR group ($n = 10$) for patients with the triple-negative subtype (13.8% ± 6.5 vs 49.6% ± 29.2, $P = .004$) (Table 3). The area under the ROC curve for PRM_{SI+} in the prediction of pCR was 0.770 (95% confidence interval: 0.626, 0.879), with a best PRM_{SI+} cutoff value of 20.8% that yielded 100% (six of six pCR) sensitivity and 71% (30 of 42 npCR) specificity (Fig 4a). The area under the ROC curve for PRM_{SI+} in the prediction of a good response was 0.716 (95% confidence interval: 0.567, 0.837), with a best PRM_{SI+} cutoff value of 28.6% that yielded 55% (21 of 38 good responses) sensitivity and 90% (nine of 10 minor responses) specificity (Fig 4b). The best cutoff determined with the leave-one-out cross validation was 20.8%, the same with the best cutoff point determined with maximal sum of the sensitivity and specificity values according to ROC analysis in the prediction of pCR and npCR groups. However, the cutoff

Table 2

Association between Imaging Variables and Pathologic Response

Variable	pCR ($n = 6$)	npCR ($n = 42$)	*P* Value	Good Response ($n = 38$)	Minor Response ($n = 10$)	*P* Value
Mean tumor size						
Baseline (cm)			.888			.506
Mean ± SD*	4.9 ± 1.8 (2.6–7.4)	5.0 ± 2.0 (1.5–11.5)		5.1 ± 2.0 (1.5–11.5)	4.6 ± 2.0 (2.4–9.2)	
Median†	4.7 (3.7–6.0)	4.5 (3.8–5.9)		4.8 (3.9–6.2)	3.9 (3.4–5.2)	
After the first NAC (cm)			.695			.824
Mean ± SD*	4.2 ± 1.8 (2.0–6.4)	4.5 ± 1.8 (1.2–9.2)		4.5 ± 1.8 (1.2–8.3)	4.3 ± 2.0 (2.4–9.2)	
Median†	4.2 (2.8–5.6)	4.3 (3.5–5.7)		4.4 (3.3–5.7)	3.6 (3.1–5.1)	
Percentage change in tumor size			.3			.178
Mean ± SD*	−15.3 ± 12.5 (−30.8 to 3.2)	−9.7 ± 12.2 (−34.8 to 26.7)		−11.7 ± 13.1 (−34.8 to 26.7)	−6.8 ± 7.2 (−16.1 to 2.9)	
Median†	−17.0 (−23.1 to −8.2)	−7.5 (−17.9 to −0.5)		−8.7 (−21.7 to −2.2)	−3.8 (−11.3 to −0.5)	
Mean tumor volume						
Baseline (cm^3)			.651			.967
Mean ± SD*	22.0 ± 18.7 (1.3–46.2)	38.9 ± 89.8 (0.8–552.3)		36.6 ± 90.6 (0.8–552.3)	37.6 ± 58.1 (5.6–196.1)	
Median†	18.7 (7.7–36.8)	14.1 (6.0–23.5)		12.5 (5.8–26.5)	16.3 (9.6–27.9)	
After the first NAC (cm^3)			.407			.726
Mean ± SD*	11.0 ± 13.2 (1.0–36.7)	26.4 ± 44.4 (0.73–232.6)		23.4 ± 43.4 (0.7–232.6)	28.4 ± 38.2 (4.5–127.1)	
Median†	8.2 (2.9–10.0)	11.8 (4.5–23.1)		9.8 (3.2–20.4)	14.1 (7.7–23.6)	
Percentage change in tumor volume			.309			.965
Mean ± SD*	−38.7 ± 46.0 (−85.6 to 20.8)	−14.1 ± 55.9 (−79.8, 287.6)		−17.0 ± 61.5 (−85.6 to 287.6)	−17.9 ± 14.1 (−42.6 to 5.2)	
Median†	−47.7 (−75.9 to −2.2)	−20.5 (−37.7, −4.7)		−23.6 (−44.0 to −1.4)	−15.3 (−25.9 to −9.7)	
PRM between baseline and after the first NAC (%)						
PRM_{SI+}			<.001			.041
Mean ± SD*	14.0 ± 6.5 (5.6–20.8)	40.7 ± 27.2 (0.7–89.8)		34.3 ± 26.4 (0.7–89.8)	52.8 ± 24.9 (2.3–82.8)	
Median†	14.4 (9.0–19.7)	39.5 (19.3–62.9)		27.0 (12.0–53.7)	58.1 (39.4–68.2)	
PRM_{SI-}			<.001			.04
Mean ± SD*	83.4 ± 7.6 (74.5–93.2)	56.4 ± 27.8 (8.0–99.1)		64.0 ± 26.9 (8.0–99.1)	43.9 ± 25.6 (13.5–97.4),	
Median†	83.2 (77.2–89.1)	57.1 (32.8–77.7)		69.2 (43.0–86.0)	38.0 (28.5–57.6)	
PRM_{SI0}			.739			
Mean ± SD*	2.7 ± 1.4 (1.3–4.9)	2.9 ± 1.5 (0.2–5.6)		2.7 ± 1.4 (0.2–5.3)	3.3 ± 1.6 (0.3–5.6)	.315
Median†	2.5 (1.6–3.2)	3.1 (1.8–4.1)		2.9 (1.5–3.5)	3.4 (2.4–4.3)	
K^{trans}						
Baseline (min^{-1})			.785			.327
Mean ± SD*	0.263 ± 0.044 (0.196–0.329)	0.254 ± 0.080 (0.033–0.408)		0.249 ± 0.078 (0.033–0.397)	0.276 ± 0.069 (0.205–0.408)	
Median†	0.267 (0.246–0.277)	0.249 (0.204–0.296)		0.253 (0.196–0.290)	0.264 (0.219–0.305)	
After the first NAC (min^{-1})			.759			.336
Mean ± SD*	0.224 ± 0.076 (0.108–0.309)	0.234 ± 0.068 (0.069–0.369)		0.227 ± 0.074 (0.069–0.369)	0.251 ± 0.043 (0.192–0.326)	

Table 2 (continues)

Table 2 (continued)

Association between Imaging Variables and Pathologic Response

Variable	pCR ($n = 6$)	npCR ($n = 42$)	*P* Value	Good Response ($n = 38$)	Minor Response ($n = 10$)	*P* Value
Median†	0.230 (0.185–0.280)	0.229 (0.201–0.291)		0.222 (0.184–0.291)	0.243 (0.230–0.285)	
Percentage change in mean K^{trans}			.609			.626
Mean ± SD*	−15.9 ± 21.2 (−55.4 to 7.6)	20.8 ± 72.0 (−71.0 to 101.8)		22.3 ± 82.6 (−71.0 to 101.8)	−6.3 ± 16.9 (−31.6 to 20.6)	
Median†	−12.2 (−15.9 to −7.5)	−6.5 (−30.7 to 7.4)		−11.6 (−33.2 to 5.4)	−8.1 (−17.5 to 6.9)	
k_{ep}						
Baseline (min^{-1})			.575			.339
Mean ± SD*	0.616 ± 0.262 (0.448–1.138)	0.787 ± 0.729 (0.294–4.067)		0.816 ± 0.754 (0.330–4.067)	0.579 ± 0.315 (0.294–1.375)	
Median†	0.535 (0.463–0.584)	0.540 (0.406–0.726)		0.561 (0.442–0.736)	0.466 (0.400–0.643)	
After the first NAC (min^{-1})			.363			.459
Mean ± SD*	0.992 ± 0.917 (0.346–2.781)	0.616 ± 0.298 (0.233–1.787)		0.696 ± 0.486 (0.233–2.781)	0.577 ± 0.225 (0.336–1.003)	
Median†	0.680 (0.437–1.002)	0.536 (0.406–0.775)		0.579 (0.423–0.809)	0.530 (0.394–0.712)	
Percentage change in mean k_{ep}			.241			.774
Mean ± SD*	46.1 ± 74.4 (−34.3 to 144.4)	6.3 ± 76.3 (−82.0 to 276.2),		9.9 ± 79.0 (−82.0 to 276.2)	18.0 ± 70.7 (−56.9 to 184.9)	
Median†	38.8 (−16.1 to 102.0)	−12.8 (−41.7 to 18.2)		−12.8 (−41.7 to 39.9)	−0.4 (−23.8 to 25.1)	
v_e						
Baseline			.831			.243
Mean ± SD*	0.563 ± 0.129 (0.352–0.669)	0.550 ± 0.146 (0.071–0.778)		0.538 ± 0.146 (0.071–0.753)	0.598 ± 0.121 (0.417–0.778)	
Median†	0.599 (0.502–0.667)	0.592 (0.457–0.639)		0.579 (0.457–0.653)	0.610 (0.524–0.651)	
After the first NAC			.141			.179
Mean ± SD*	0.467 ± 0.151 (0.271–0.708)	0.557 ± 0.136 (0.274–0.908)		0.529 ± 0.146 (0.271–0.908)	0.597 ± 0.109 (0.469–0.802)	
Median†	0.483 (0.378–0.504)	0.553 (0.491–0.647)		0.535 (0.463–0.644)	0.590 (0.502–0.650)	
Percentage change in mean v_e			.485			.594
Mean ± SD*	−13.9 ± 32.1 (−48.4 to 35.5)	27.0 ± 40.3 (−56.6 to 83.4)		27.3 ± 49.5 (−56.6 to 83.4)	1.6 ± 16.6 (−26.7 to 25.0)	
Median†	−16.0 (−39.7 to 2.8)	3.1 (−15.5 to 20.6)		−0.2 (−23.9 to 21.3)	5.6 (−12.0 to12.5)	

* Numbers in parentheses are ranges. SD = standard deviation.

† Numbers in parentheses are interquartile ranges.

Figure 3

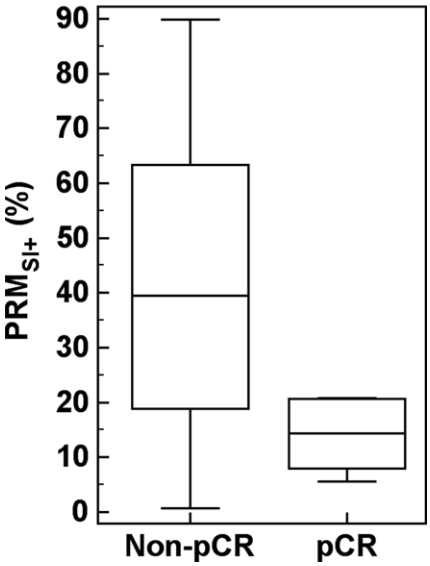

Figure 3: Box and whisker plot of the PRM$_{SI+}$ after the first cycle of chemotherapy in the npCR and pCR groups. Top of each box = 25th percentile of the SI values, bottom of each box = 75th percentile of the SI values, horizontal line inside each box = median value. The mean PRM of the proportion of voxels with increased SI of the npCR group was significantly higher than that of the pCR group (40.7% ± 27.2 vs 14.0% ± 6.5, $P < .001$).

by using the leave-one-out cross validation in the prediction of good response and minor response groups was 40.5%, which was different from the best cutoff of 28.6% determined by using the maximal sum of the sensitivity and specificity values.

Discussion

Our data showed that the results of volumetric voxel-based analysis of changes in SI after the first cycle of NAC are associated with subsequent pathologic response after surgery.

Our results are consistent with data in reports in which Gálban et al (9,10) found that a large number of voxels with increased relative cerebral blood volume in the PRM and decreased relative cerebral blood volume in the PRM within the tumor volume of high-grade glioma was highly predictive of poor survival, whereas standard ROI analysis relying on the mean value of the whole tumor did not effectively help predict survival. In contrast to the studies of Gálban et al (9,10), we compared the PRM findings using the SI change and the mean value of the conventional ROI measurements of K^{trans}, k_{ep}, and v_e within the tumor. Although the Translational Research Working Group of the National Cancer Institute recommends the use of K^{trans}, k_{ep}, and v_e for clinical trials (26), this is a labor-intensive technique. Given the correlation between PRM findings obtained according to SI changes and the pathologic response observed in our study, it is likely that PRM analysis is sufficiently sensitive to help detect the early microvascular changes produced by NAC. The higher PRM$_{SI+}$ found in the npCR group can probably be explained by the inability of the therapy to interrupt tumor vasculature, thus leading to tumor growth. According to our findings (which will need confirmation from a prospective larger study), when patients with breast cancer manifest a PRM$_{SI+}$ lower than 20.8% after the first cycle of chemotherapy, the NAC regimen can be completed with confidence (100% [six of six pCR] sensitivity). In contrast, when patients manifest a PRM$_{SI+}$ higher than 28.6%, we expect that these patients will not respond to NAC (90% [nine of 10 minor responses] specificity) and can therefore be directed to alternative therapy, thereby avoiding the toxicity of ineffective chemotherapy.

Our finding of the lack of significant differences in tumor volume change or pharmacokinetic parameters between the pCR and npCR groups contrasts with findings from recent studies. For example, American College of Radiology Imaging Network 6657 reported that tumor volume changes after the first cycle of chemotherapy were more effective for the prediction of pCR than tumor diameter, signal enhancement ratio, or clinical size (8). Our inability to observe a significant difference may be related to the relatively small number of patients in our study. A recent systematic review (27) of the accuracy of breast MR imaging suggested that K^{trans} demonstrated the highest sensitivity and specificity in the early prediction of pathologic response. It is likely that the timing of the sequential MR examination contributed to the discrepancy in these results. Ah-See et al (5) performed MR examinations following the second cycle of chemotherapy, whereas we performed the MR examination following the first cycle of chemotherapy when the tumors showed less of a size reduction and K^{trans} or k_{ep} did not demonstrate predictive power. Moreover, researchers in an earlier study (28) also reported the lack of a significant difference in K^{trans} between responders and nonresponders after the first cycle of chemotherapy at a median of 21 days (range, 16–22 days) after the first cycle, which is similar to our median interval of 21 days (range, 13–36 days). In addition, the K^{trans} or k_{ep} in our study ranged from 0.2–0.5, with a standard deviation of 0.1–0.3, and 0.8–1.2, with a standard deviation of 0.2–0.5, respectively, which were within similar parameter ranges reported in previous studies (6,29).

With regard to immunohistochemical subtype, investigators in a recent study suggested that pCR was more predictive of recurrence-free survival when the subtype was considered (30). In hormone receptor–positive tumors, pCR after chemotherapy demonstrated no substantial prognostic value, as the pCR rate was low and residual disease should be expected (31). In our study, pCR was observed slightly more frequently (29%, four of 14) for the triple-negative subtype than the hormone receptor–positive (4%, one of 27) or *HER2*-positive (14%, one of seven) subtypes but significance was not achieved, possibly because of small sample size (P = .073). In addition, an association between PRM findings and pCR was also found for the triple-negative subtype. Thus, in future studies of imaging biomarkers in breast cancer patients in the NAC setting, the molecular subtype should be considered.

The strengths of our study include its prospective design, use of a consistent MR imaging protocol, consistent timing of imaging to evaluate early

Table 3

Association between PRM and Pathologic Response According to Subtype

Variable	pCR Group ($n = 6$)	npCR Group ($n = 42$)	*P* Value	Good Response Group ($n = 38$)	Minor Response Group ($n = 10$)	*P* Value
Triple negative						
PRM_{SI+}	3.8 ± 6.5*	49.6 ± 29.2†	.004	29.7 ± 28.4†	63.4 ± 18.1*	.051
PRM_{SI-}	83.5 ± 8.1*	47.3 ± 29.9†	.005	67.5 ± 28.9†	33.1 ± 19.2*	.051
PRM_{SI0}	2.7 ± 1.7*	3.1 ± 1.5†	.705	2.8 ± 1.6†	3.5 ± 1.5*	.429
Hormone receptor positive						
PRM_{SI+}	8.0‡	37.9 ± 26.6§	NA	35.6 ± 25.4‖	46.6 ± 40.8#	.511
PRM_{SI-}	89.9‡	59.4 ± 27.2§	NA	61.6 ± 26.1‖	51.6 ± 41.8#	.561
PRM_{SI0}	2.2‡	2.7 ± 1.5§	NA	2.8 ± 1.4‖	1.8 ± 1.5#	.264
HER2 positive						
PRM_{SI+}	20.8‡	37.9 ± 28.2**	NA	28.4 ± 33.0*	44.9 ± 15.9#	.468
PRM_{SI-}	76.3‡	58.8 ± 28.5**	NA	69.2 ± 32.8*	50.7 ± 15.9#	.417
PRM_{SI0}	2.9‡	3.3 ± 1.4**	NA	2.4 ± 1.1*	4.4 ± 0.1#	.032

Note.—NA = not applicable.

* Data are means ± standard deviations, with $n = 4$.

† Data are means ± standard deviations, with $n = 10$.

‡ Data are PRM values of the case, with $n = 1$.

§ Data are means ± standard deviations, with $n = 26$.

‖ Data are means ± standard deviations, with $n = 24$.

Data are means ± standard deviations, with $n = 3$.

** Data are means ± standard deviations, with $n = 6$

Figure 4

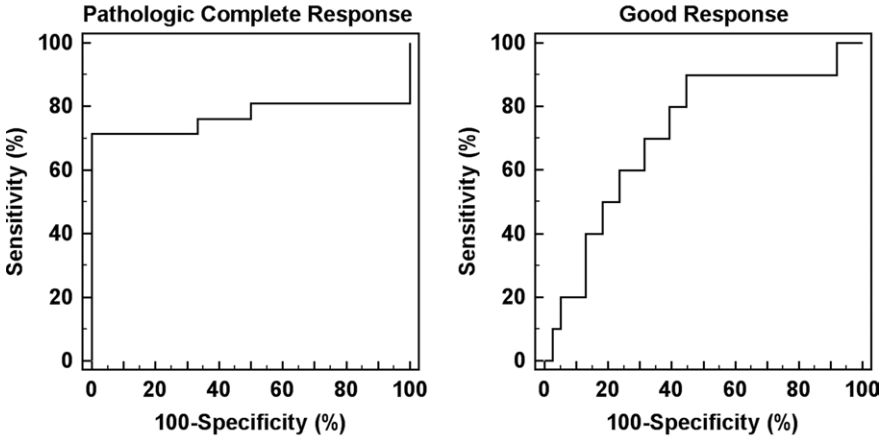

a. b.

Figure 4: ROC curves for the PRM_{SI+} after the first cycle of chemotherapy in the prediction of **(a)** pCR or **(b)** good response in 48 patients with breast cancer.

predictability, consistent chemotherapy regimen, PRM and pharmacokinetic analyses obtained for the same population, and the practical applicability of the results.

However, our study had some limitations. First, the a priori determination of the appropriate patient number for sample size was 52; however, because of the higher than expected number of dropouts, our study only had a final study population of 48. Second, as PRM analysis requires similar images before and after chemotherapy for intra- and interstudy registration, we used nonlinear semiautomatic software for registration and could not evaluate the accuracy of registration. Because of tumoral heterogeneity, particularly after the first cycle of chemotherapy, small changes of a shift of 1 to 3 pixels might have affected the results. Third, we did not evaluate the reproducibility of DCE MR imaging with PRM analysis. However, high reproducibility of the software used for tumor segmentation in DCE MR imaging was reported in a previous study (32). Last, the cutoff values for MR imaging parameters determined for our population may have led to overestimation of our results. Therefore, a large study with a validation cohort is warranted for future research.

In conclusion, PRM analysis of SI changes on DCE MR images may provide early identification of pathologic responsiveness to NAC and may be used as a biomarker of tumor response in patients with breast cancers who are undergoing NAC.

Disclosures of Conflicts of Interest: N.C. disclosed no relevant relationships. **S.A.I.** disclosed no relevant relationships. **I.A.P.** disclosed no relevant relationships. **K.H.L.** disclosed no relevant relationships. **M.L.** disclosed no relevant relationships. **W.H.** disclosed no relevant relationships. **D.Y.N.** disclosed no relevant relationships. **W.K.M.** disclosed no relevant relationships.

References

1. Rastogi P, Anderson SJ, Bear HD, et al. Preoperative chemotherapy: updates of National Surgical Adjuvant Breast and Bowel Project Protocols B-18 and B-27. J Clin Oncol 2008;26(5):778–785.
2. van der Hage JA, van de Velde CJ, Julien JP, Tubiana-Hulin M, Vandervelden C, Duchateau L. Preoperative chemotherapy in primary operable breast cancer: results from the European Organization for Research and Treatment of Cancer trial 10902. J Clin Oncol 2001;19(22):4224–4237.
3. Kaufmann M, von Minckwitz G, Mamounas EP, et al. Recommendations from an international consensus conference on the current status and future of neoadjuvant systemic therapy in primary breast cancer. Ann Surg Oncol 2012;19(5):1508–1516.
4. Bear HD, Anderson S, Smith RE, et al. Sequential preoperative or postoperative docetaxel added to preoperative doxorubicin plus cyclophosphamide for operable breast cancer:National Surgical Adjuvant Breast and Bowel Project Protocol B-27. J Clin Oncol 2006;24(13):2019–2027.
5. Ah-See ML, Makris A, Taylor NJ, et al. Early changes in functional dynamic magnetic resonance imaging predict for pathologic response to neoadjuvant chemotherapy in primary breast cancer. Clin Cancer Res 2008;14(20):6580–6589.
6. Yu Y, Jiang Q, Miao Y, et al. Quantitative analysis of clinical dynamic contrast-enhanced MR imaging for evaluating treatment response in human breast cancer. Radiology 2010;257(1):47–55.
7. Li SP, Makris A, Beresford MJ, et al. Use of dynamic contrast-enhanced MR imaging to predict survival in patients with primary breast cancer undergoing neoadjuvant chemotherapy. Radiology 2011;260(1):68–78.
8. Hylton NM, Blume JD, Bernreuter WK, et al. Locally advanced breast cancer: MR imaging for prediction of response to neoadjuvant chemotherapy—results from ACRIN 6657/I-SPY TRIAL. Radiology 2012;263(3):663–672.
9. Galbán CJ, Chenevert TL, Meyer CR, et al. The parametric response map is an imaging biomarker for early cancer treatment outcome. Nat Med 2009;15(5):572–576.
10. Galbán CJ, Chenevert TL, Meyer CR, et al. Prospective analysis of parametric response map-derived MRI biomarkers: identification of early and distinct glioma response patterns not predicted by standard radiographic assessment. Clin Cancer Res 2011;17(14):4751–4760.
11. Bonekamp S, Jolepalem P, Lazo M, Gulsun MA, Kiraly AP, Kamel IR. Hepatocellular carcinoma: response to TACE assessed with semiautomated volumetric and functional analysis of diffusion-weighted and contrast-enhanced MR imaging data. Radiology 2011;260(3):752–761.
12. Chou CP, Wu MT, Chang HT, et al. Monitoring breast cancer response to neoadjuvant systemic chemotherapy using parametric contrast-enhanced MRI: a pilot study. Acad Radiol 2007;14(5):561–573.
13. Keam B, Im SA, Kim HJ, et al. Clinical significance of axillary nodal ratio in stage II/III breast cancer treated with neoadjuvant chemotherapy. Breast Cancer Res Treat 2009;116(1):153–160.
14. Chatterji M, Mercado CL, Moy L. Optimizing 1.5-tesla and 3-tesla dynamic contrast-enhanced magnetic resonance imaging of the breasts. Magn Reson Imaging Clin N Am 2010;18(2):207–224.
15. Grady L. Random walks for image segmentation. IEEE Trans Pattern Anal Mach Intell 2006;28(11):1768–1783.
16. Yi A, Cho N, Im SA, et al. Survival outcomes of breast cancer patients who receive neoadjuvant chemotherapy: association with dynamic contrast-enhanced MR imaging with computer-aided evaluation. Radiology 2013;268(3):662–672.
17. Tofts PS. Modeling tracer kinetics in dynamic Gd-DTPA MR imaging. J Magn Reson Imaging 1997;7(1):91–101.
18. Tofts PS, Brix G, Buckley DL, et al. Estimating kinetic parameters from dynamic contrast-enhanced T(1)-weighted MRI of a diffusable tracer: standardized quantities and symbols. J Magn Reson Imaging 1999;10(3):223–232.
19. Rohrer M, Bauer H, Mintorovitch J, Requardt M, Weinmann HJ. Comparison of magnetic properties of MRI contrast media solutions at different magnetic field strengths. Invest Radiol 2005;40(11):715–724.
20. Fram EK, Herfkens RJ, Johnson GA, et al. Rapid calculation of T1 using variable flip angle gradient refocused imaging. Magn Reson Imaging 1987;5(3):201–208.
21. Orton MR, d'Arcy JA, Walker-Samuel S, et al. Computationally efficient vascular input function models for quantitative kinetic modelling using DCE-MRI. Phys Med Biol 2008;53(5):1225–1239.
22. Ogston KN, Miller ID, Payne S, et al. A new histological grading system to assess response of breast cancers to primary chemotherapy: prognostic significance and survival. Breast 2003;12(5):320–327.
23. Silver DP, Richardson AL, Eklund AC, et al. Efficacy of neoadjuvant cisplatin in triple-negative breast cancer. J Clin Oncol 2010;28(7):1145–1153.
24. Wolff AC, Hammond ME, Schwartz JN, et al. American Society of Clinical Oncology/College of American Pathologists guideline recommendations for human epidermal growth factor receptor 2 testing in breast cancer. J Clin Oncol 2007;25(1):118–145.
25. Faul F, Erdfelder E, Lang AG, Buchner AG. G*Power 3: a flexible statistical power analysis program for the social, behavioral, and biomedical sciences. Behav Res Methods 2007;39(2):175–191.
26. Guidelines from the National Cancer Institute Cancer Imaging Program MR Workshop on Translational Research in Cancer. http://dctd.cancer.gov/ProgramPages/cip/clinical_trials_imaging.htm. Published 2004. Accessed May 7, 2013.
27. Marinovich ML, Sardanelli F, Ciatto S, et al. Early prediction of pathologic response to neoadjuvant therapy in breast cancer: systematic review of the accuracy of MRI. Breast 2012;21(5):669–677.
28. Padhani AR, Hayes C, Assersohn L, et al. Prediction of clinicopathologic response of breast cancer to primary chemotherapy at contrast-enhanced MR imaging: initial clinical results. Radiology 2006;239(2):361–374.
29. Koo HR, Cho N, Song IC, et al. Correlation of perfusion parameters on dynamic contrast-enhanced MRI with prognostic factors and subtypes of breast cancers. J Magn Reson Imaging 2012;36(1):145–151.
30. Esserman LJ, Berry DA, DeMichele A, et al. Pathologic complete response predicts recurrence-free survival more effectively by cancer subset: results from the I-SPY 1 TRIAL—CALGB 150007/150012, ACRIN 6657. J Clin Oncol 2012;30(26):3242–3249.
31. von Minckwitz G, Untch M, Blohmer JU, et al. Definition and impact of pathologic complete response on prognosis after neoadjuvant chemotherapy in various intrinsic breast cancer subtypes. J Clin Oncol 2012;30(15):1796–1804.
32. Bauknecht HC, Romano VC, Rogalla P, et al. Intra- and interobserver variability of linear and volumetric measurements of brain metastases using contrast-enhanced magnetic resonance imaging. Invest Radiol 2010;45(1):49–56.